Ar–Ar dating of authigenic K-feldspar: Quantitative modelling of radiogenic argon-loss through subgrain boundary networks

Journal Item

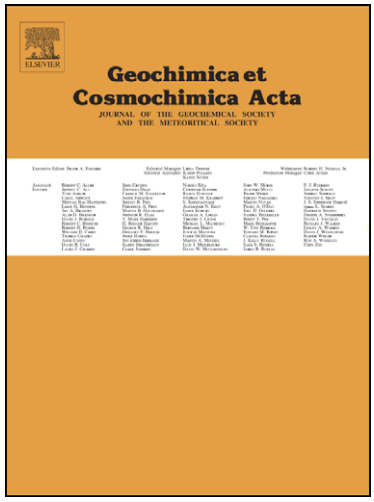

Ar-Ar dating of authigenic K-feldspar: quantitative modelling of radiogenic argon-loss through subgrain boundary networks

D.F. Mark, S.P. Kelley, M.R. Lee, J. Parnell, S.C. Sherlock, D. Brown

PII: S0016-7037(08)00171-3
DOI: 10.1016/j.gca.2008.03.018
Reference: GCA 5602

To appear in: *Geochimica et Cosmochimica Acta*

Received Date: 22 May 2007
Accepted Date: 25 March 2008

Please cite this article as: Mark, D.F., Kelley, S.P., Lee, M.R., Parnell, J., Sherlock, S.C., Brown, D., Ar-Ar dating of authigenic K-feldspar: quantitative modelling of radiogenic argon-loss through subgrain boundary networks, *Geochimica et Cosmochimica Acta* (2008), doi: 10.1016/j.gca.2008.03.018

REVISED MANUSCRIPT (W5010) SUBMITTED: 11th March 2008

Ar-Ar dating of authigenic K-feldspar: quantitative modelling of radiogenic argon-loss through subgrain boundary networks

D. F. Mark[1,2*], S. P. Kelley[3], M. R. Lee[4], J. Parnell[1], S. C. Sherlock[3] & D. Brown[4]

[1] Department of Geology & Petroleum Geology, Meston Building, Meston Walk, University of Aberdeen, Aberdeen, AB24 3UE

[2] NERC Argon Isotope Facility, Scottish Universities Environmental Research Centre, Rankine Avenue, Scottish Enterprise Technology Park, East Kilbride, G75 0QF, Scotland, UK

[3] Centre for Earth, Planetary, Space and Astronomical Research (CEPSAR), Department of Earth Sciences, Open University, Walton Hall, Milton Keynes, MK7 6AA

[4] Department of Geographical and Earth Sciences, University of Glasgow, Gregory Building, Lilybank Gardens, Glasgow, G12 8QQ

ABSTRACT

We have analysed two distinct generations of authigenic K-feldspar in Fucoid Bed sandstones from An-t-Sron and Skiag Bridge, NW Highlands, Scotland, which have experienced post-growth heating to levels in excess of the predicted Ar closure temperature. Authigenic K-feldspars show microtextural similarities to patch perthites; that is subgrains separated by dislocation rich boundary networks that potentially act as fast diffusion pathways for radiogenic argon.

The two generations of authigenic K-feldspar in the Fucoid Bed sandstones can be distinguished by different microtextural zones, bulk mineral compositions, fluid inclusion populations, and inferred temperatures and chemistries of parent fluids. Ar-Ar age data obtained using high-resolution ultraviolet laser ablation, show that the

* Corresponding author (d.mark@suerc.gla.ac.uk)

first cementing generation is Ordovician and the second cementing generation is Silurian.

Modelling of Ar-diffusion using subgrain size as the effective diffusion dimension and a simplified tectono-thermal thrust model assuming transient heating of the Fucoid Beds is inconsistent with observed data. Removal of heat from the thrust zone through rapid flushing of heated fluids rather than transient heating can be invoked to explain the observed Ar-Ar ages for both generations of cement. Alternatively, Ar-diffusion modelling using overgrowth thickness as the effective diffusion dimension instead of subgrain size also yields models that are consistent with both the Fucoid Bed palaeothermal maxima and determined Ar-Ar age ages for the two generations of K-feldspar cement. Based on this alternate explanation, we propose a theoretical microtextural model that highlights fundamental differences between the microtextures of deuterically formed patch perthites and authigenic K-feldspars, explaining the apparent robustness of authigenic K-feldspar with respect to Ar-retention.

KEYWORDS

Authigenic K-feldspar, Ar diffusion, FIB-TEM, Ar-Ar, subgrain, microtexture

1. INTRODUCTION

1.1 Alkali K-feldspar

The abundance of K-feldspar in igneous rocks and its occurrence as detrital and authigenic constituents in sedimentary rocks, has ensured its extensive use in Ar-Ar dating (McDougall & Harrison, 1999). Step heating experiments (Burgess *et al.*, 1992; Parsons, 1994) show that Ar-Ar dates obtained from plutonic and detrital K-feldspars reflect the age of cooling below the Ar closure temperature (T_c). T_c is simply one temperature range in a range of temperatures (a closure 'interval') in the cooling history of a rock that corresponds to its apparent age (Lee, 1995).

Patch perthite microtextures are key indicators of interaction of alkali feldspar with deuteric fluids and are characterised by mosaics of slightly misaligned submicron- to micron-sized incoherent subgrains with abundant dislocations along their boundaries and are also typically associated with micropores (Foland, 1994; Parsons & Lee, 2005; Walker *et al.*, 1995: Fig. 1). Combined Ar-Ar geochronology and transmission electron microscope (TEM) studies suggest that Ar-loss from alkali feldspar is controlled directly by subgrain microtextures (Parsons, 1978; Worden *et al.*, 1990; Burgess *et al.*, 1992; Parsons & Lee, 2000; Lee & Parsons, 2003; Parsons & Lee., 2005).

1.2 Authigenic K-feldspar

Although step heating experiments originally designed to determine the age of authigenic K-feldspar overgrowths (Hearn & Sutter, 1985; Hearn *et al.*, 1987; Girard *et al.*, 1988; Spotl *et al.*, 1996; Warnock & van der Kamp, 1999; Liu *et al.*, 2003) have not directly enabled the distinction between detrital and authigenic generations, the data suggest that authigenic K-feldspar may record isotopic information relating to

diagenetic events. The introduction of laserprobe isotope extraction techniques has offered higher-spatial resolution than conventional methods, permitting Ar-extraction from individual grains and potentially eliminating problems of contamination from detrital feldspar. Initial laserprobe studies used Ar-ion and infrared laser systems for analysis of authigenic K-feldspar (Walgenwitz *et al*., 1990). Laser absorption by feldspar at such wavelengths is poor, however, and extensive heating occurred outside the site of laser-mineral interaction, resulting not only in the extraction of Ar from the overgrowth, but also from the detrital grain and surrounding minerals. The ultraviolet (UV, 266 nm) laserprobe (Kelley *et al*., 1994) has a greater spatial resolution than the Ar-ion and infrared laser systems (UV laser can achieve a spot resolution of 12 μm) and the wavelengths are absorbed strongly by the feldspar. As a consequence the UV laser does not heat the sample beyond the point of laser-sample interaction and therefore only extracts Ar from the desired locations. Investigations dating K-feldspar overgrowths using the UV laserprobe have yielded meaningful Ar-Ar growth ages (Hagen *et al*., 2001; Mark *et al*., 2005, 2008; Sherlock *et al*., 2005).

Authigenic K-feldspar overgrowths within sedimentary rocks from the Permo-Triassic of Elgin (Worden & Rushton, 1992), the Jurassic Humber Group of the North Sea (Lee & Parsons, 2003) and the Cretaceous Atlantic Margin Victory Formation (Mark *et al*., 2005), all show mineralogical and microtextural similarities. These overgrowths comprise mosaics of slightly misaligned submicron- to micron-sized subgrains, intercalated micropores, and nanometre growth bands orientated parallel to dislocation-rich subgrain boundaries. Overgrowths from Elgin and the Victory Formation have a regular subgrain size and well-developed crystal faces dominated by the {110} adularia habit. Subgrain boundaries of overgrowths from the Humber

Group are slightly curved with the {110} adularia habit. Subgrain size also increases with distance from the detrital grain-overgrowth interface. The presence of illite along subgrain boundaries at interfaces was noted in two studies (Worden & Rushton, 1992; Lee & Parsons, 2003).

Ar-Ar dating of authigenic K-feldspar is contentious because subgrain microtextures are superficially similar to those of deuterically formed patch perthites (Lee & Parsons, 2003) which quantitatively leak Ar at low temperatures (Burgess *et al.*, 1992). However, because subgrains can be equated to spherical Ar diffusion domains it is possible to model Ar-loss (Wheeler, 1996) by assuming that Ar diffuses out of the subgrains via lattice volume diffusion to an infinite zero concentration reservoir. The effective diffusion domain (sphere diameter) is directly related to T_c; the larger the diffusion domain the higher the T_c (Dodson, 1973). Therefore, because authigenic K-feldspar microtextures are superficially similar to those of patch perthites, it has been logically suggested that authigenic K-feldspar will leak Ar at relatively low temperatures, with the initial temperature of Ar-loss being related directly to the radius of the smallest subgrain (Lee & Parsons, 2003).

Sherlock *et al*. (2005) modelled the thermal response of authigenic K-feldspar to an episode of tectonically induced heating. Because TEM was not used to characterise microtextures, the model was generic and covered a wide range of subgrain sizes but demonstrated that authigenic K-feldspar can potentially retain Ar. The first fully quantitative study of authigenic K-feldspar incorporating Ar diffusion modelling, Ar-Ar geochronology and TEM (Mark *et al*., 2005), modelled subgrain response in terms of Ar-loss against a thermal burial history that was reconstructed using apatite fission

130 track analysis, fluid inclusion microthermometry and vitrinite reflectance. The model
131 showed that 3 to 5 μm subgrains exposed to a maximum temperature of 125 °C for ~
132 10 Ma, yielded meaningful Ar-Ar growth ages. Predicted closure temperature
133 estimates for sugrains of such sizes range from ~ 150 to 175 °C (Foland, 1974, 1994).
134
135 A key question which this study aims to address is the difference between the Ar-
136 retention properties of deuterically formed patch perthites within alkali feldspars (Fig.
137 1) and authigenic K-feldspar overgrowths. As these microtextures are superficially
138 similar, how do their Ar-diffusion properties compare?
139
140 1.3 Study aims
141
142 This study attempts to determine if Ar is quantitatively retained by authigenic K-
143 feldspar overgrowths when exposed to temperatures in excess of predicted T_c
144 determined from the calculations of Dodson (1973) and Foland (1974, 1994). Ar-Ar
145 geochronology, TEM imaging and electron diffraction and Ar-diffusion modelling
146 were employed to constrain the subgrain response of authigenic K-feldspar to
147 temperatures in the order of 200 ˚C. A Focused Ion Beam (FIB) technique (Lee *et al*.,
148 2003) was used to cut electron-transparent foils from precisely located areas of K-
149 feldspar crystals within polished thin sections. Comparison of subgrain microtexture
150 revealed by TEM with Ar-Ar data enabled the simulation of Ar-diffusion domains and
151 subsequently, the data were modelled against a post-crystallization, orogenesis-driven
152 tectono-thermal episode, hence constraining the reliability of the Ar-Ar ages. Fine-
153 grained sandstone samples were collected from Fucoid Bed outcrops at An-t-Sron and
154 Skiag Bridge, NW Highlands, two sites that are geographically 30 km apart (Fig. 2).

A documented enrichment of K-feldspar, up to 12 wt. % K_2O (Bowie *et al*., 1966) has been reported in the lower part of the Lower Cambrian An-t-Sron Formation (Fucoid Beds) thus providing an ideal geological context for assessing the retentiveness of authigenic K-feldspar with respect to Ar. This manuscript should be considered as a companion to Mark *et al*. (2007).

2. GEOLOGICAL SETTING

The Fucoid Beds were deposited between 518 and 510 Ma (Gradstein *et al*., 2004) on the Laurentian Platform, and consist of up to 27 m of siltstones with interbedded sandstones and dolostones. These rocks crop out along the Moine Thrust Zone and were a focus for deformation during closure of the Iapetus Ocean. The Moine Supergroup was thrust onto the Cambrian-Ordovician succession during the Scandian episode (435-420 Ma; Dewey, 2005) of the Caledonian Orogeny (a continent-continent collision that produced a mountain range of similar scale to the active Himalaya; Johnson *et al*., 1985). Thrusting disturbed the geothermal gradient of this region and equilibrium was restored by conductive heat transport from the thrust sheet to the underlying Cambrian-Ordovician sequence (Oxburgh & Turcotte, 1974). It has been estimated from acritarch coloration index (Downie, 1982), fluid inclusion studies (Baron *et al*., 2003; Mark *et al*., 2007) and illite crystallinity analyses (Johnson *et al*., 1985) that temperatures in the sampled sections of the Fucoid Beds reached a temperature of 200 °C, the sampled regions palaeothermal maxima.

3. METHODS (*SMALL TEXT IN MANUSCRIPT*)

3.1 Excision of electron transparent foils using the focused ion beam technique

Sites within the K-feldspar overgrowths to be sampled for TEM work were selected by backscattered electron imaging of carbon coated polished thin sections using a FEI Quanta 200 field-emission scanning electron microscope (SEM) operated at 20 kV in high vacuum mode. Qualitative X-ray analyses of micrometer-sized spots were also obtained using an EDAX Pegasus 2000 energy dispersive spectrometer (EDS) microanalysis system attached to the Quanta SEM. Prior to cutting the electron-transparent foils using the Focused Ion Beam (FIB) instrument the thin sections were sputter coated with ~40 nm of gold to alleviate charging. The FIB work used a FEI 200 TEM operated at 30 kV. The milling process is described briefly below but in more detail by Heaney *et al*. (2001) and Lee *et al*. (2003). Prior to cutting of each foil a 1 µm thick platinum strip was deposited over the area of interest to protect it from damage by the Ga^+ ion beam. A pair of parallel trenches ~10 to 15 µm in length by ~ 5 µm in depth were then excavated on either side of the strip to eventually leave a ~ 110 nm thick slice of feldspar remaining between them (Fig. 3). This electron-transparent foil of the K-feldspar overgrowth (Fig. 3C, D) was then extracted from the grain using an *ex-situ* micromanipulator and placed on a 3.05 mm diameter perforated carbon film for TEM study (Fig. 3E).

3.2 High-resolution petrography

Each of the FIB-produced foils was examined initially using the Quanta SEM equipped with a secondary transmission electron microscope (STEM) detector (Fig. 3E), which enables images to be formed using electrons that have been transmitted through the thin sample (Smith *et al*., 2006). Bright-field STEM images are formed from un-scattered electrons using an electron detector positioned directly beneath the thin slice whereas dark-field images are formed from high angle scattered electrons using an offset detector. Diffraction-contrast TEM images were subsequently acquired using a FEI T20 instrument operated at 200 kV and equipped with a charge-coupled device (CCD) camera for digital image capture.

3.3 Ar-Ar ultra-violet laser ablation dating

Prior to irradiation, the two 100 µm thick doubly polished fluid inclusion wafers were cleaned ultrasonically in methanol and deionised water. Samples were cadmium shielded and irradiated for 25 (An-t-Sron) and 33 (Skiag Bridge) hours in the Canadian McMaster reactor. Neutron flux was monitored with biotite standard GA1550 (~ 98.8 ± 0.5 Ma; Renne *et al*., 1998); calculated J values of 0.00639 ± 0.000032 (An-t-Sron) and 0.01398 ± 0.00007 (Skiag Bridge) were used. A New Wave Research UP-213 nm pulsed Nd-YAG laser with a 12 µm spot size was used for Ar extraction. Due to their small size entire K-feldspar overgrowths had to be ablated in order to extract approximately ten times the blank ^{40}Ar levels. Extracted gases were cleaned using three SAES AP10 getters, two operated at 450 °C and one at room temperature. A Map 215-50 noble gas mass spectrometer analysed Ar isotope compositions. The data were corrected for blanks, mass spectrometric discrimination, ^{37}Ar decay and reactor induced interferences. Quoted Ar-Ar errors are 2σand include a 0.5 % error (including lateral variation in the flux gradient) assigned to the J value. Reactor induced correction factors used were: $(^{39}Ar/^{37}Ar)_{Ca}$ = 0.00065, $(^{36}Ar/^{37}Ar)_{Ca}$ = 0.000264, $(^{40}Ar/^{39}Ar)_{K}$ = 0.0085. Mark *et al*. (2006) provides details concerning the integration of fluid inclusion and Ar-Ar data.

3.4 Ar-diffusion modelling

Thermal history data was input into a finite element diffusion model DIFFARG (Wheeler, 1996) which works with MATLAB® software. The programme allows modelling of a precise thermal history. Effective diffusion domain size can be inputted for a series of geometry shapes and their response to the thermal history over time can be tested. DIFFARG is a forward modelling programme and hence, 0 Ma corresponds to the time of K-feldspar authigenesis. The model yields the amount of age resetting in Ma from which we determined by re-arrangement of the Ar-Ar age equation how much radiogenic Ar has been lost.

4. RESULTS

4.1 Generations of authigenic K-feldspar

241

242 Mark *et al*. (2007) show that the two generations of authigenic K-feldspar within the
243 Fucoid Beds can be resolved (prior to Ar-Ar dating) by optical and scanning electron
244 microscopy, quantitative mineral compositions, fluid inclusion petrography and parent
245 fluid temperature and chemistry throughout the whole 180 km Fucoid Bed outcrop.
246 Generation 1 cements ($P1_C$) comprise 10 to 40 µm sized overgrowths that envelop
247 detrital alkali feldspar grains whereas generation 2 cements ($P2_C$) enclose $P1_C$ and
248 occlude remaining porosity (Fig. 3A).

249

250 4.2 Authigenic K-feldspar microtextures

251

252 Foils for TEM study were cut (in samples from both An-t-Sron and Skiag Bridge)
253 using the FIB from the detrital grain-$P1_C$ interface, $P1_C$ cement, and $P2_C$ cement (Fig.
254 3B; the fourth foil removed from trench 1 in Fig. 3B was destroyed during extraction).
255 $P1_C$ and $P2_C$ are microtexturally distinct, in line with the contrasting properties of
256 their fluid inclusion populations (Mark *et al*., 2007). The microtexture of $P1_C$ feldspar
257 changes with distance from its interface with the detrital grain (Fig. 4). Proximal to
258 the interface (trench 2), the feldspar is free of subgrains and micropores and has a low
259 defect density (Fig. 4A). Further from the interface in trench 3 the $P1_C$ feldspar
260 contains 2 to 3 µm sized subgrains whose boundaries are delineated by long and
261 narrow micropores (Fig. 4B). Aggregates of a very fine (< 0.2 µm) and poorly
262 crystalline mineral occur within the micropores along subgrain boundaries, but could
263 not be identified unambiguously; their habit is suggestive of illite (Fig. 4c). By
264 contrast, the $P2_C$ feldspar (trench 4) comprises a mosaic of 0.5-1 µm sized subhedral
265 to euhedral subgrains elongate approximately parallel to b* and the euhedral

subgrains have the {110} adularia habit (Fig. 4D). Subgrain boundaries are decorated with dislocations that have an average spacing along the boundary of ~30 nm (Fig. 4E, F) and associated with micropores whose outlines are again parallel to {110} (Fig. 4E) and whose origins are inferred to be related to crystal nucleation and growth (Worden & Rushton, 1992). All of the K-feldspar has a diffuse mottling (Fig. 4F) that is characteristic of adularia. Measurements from selected area electron diffraction (SAED) patterns show that the reciprocal cell angle of this cement (y*, or 'triclinicity', which is sensitive to Si, Al order-disorder) is 90.7° and value of d_{010}/d_{100} (which is sensitive to composition) is 1.72. These values are similar to those of overgrowths in Permo-Triassic sandstones studied by Worden and Rushton (1992). $P1_C$ and $P2_C$ from both An-t-Sron and Skiag Bridge display comparable microtextures.

4.3 Ar-Ar geochronology

All Ar-Ar data are reported as 2σ throughout this manuscript. Ar-Ar ages (Ar-Ar age data tables presented in Mark *et al*., 2007) from the detrital alkali feldspars range from 518 ± 19.7 to 926 ± 51.7 Ma (n = 9). This variability is potentially a result of a combination of factors including loss of radiogenic Ar ($^{40}Ar^*$), deuteric alteration during cooling of their parent rock, natural variation in feldspar source regions and diagenetic alteration during burial. Due to these factors it was not possible to accurately constrain the source regions of the detrital K-feldspar grains. The interfaces between detrital grains and the $P1_C$ overgrowths were optically identifiable and avoided during laser ablation by leaving a 10 µm boundary between the interface and

ablation areas. Hence, the older detrital feldspar component did not contaminate the ages of the younger K-feldspar overgrowths.

Ar-Ar ages from optically identified $P1_C$ cement (entire $P1_C$ overgrowths were ablated in an attempt to maximise the extraction of Ar from the sample and minimise Ar-Ar age error) range from 450.3 ± 8.7 to 490.3 ± 14.0 Ma at An-t-Sron (n=24; Fig. 5) and 458.0 ± 26.1 to 490.2 ± 14.8 Ma at Skiag Bridge (n=15; Fig. 5). The interface between $P1_C$ and $P2_C$ cements was also optically identifiable. A 10 µm boundary was left on both sides of the $P1_C$ and $P2_C$ boundary to ensure there was no contamination during laser ablation. Ar-Ar ages from the $P2_C$ cements (entire zones of $P2_C$ cement, on average ~50 μm^2, were also ablated to minimise Ar-Ar age error) are 413.1 ± 15.0 to 450.4 ± 14.4 Ma at An-t-Sron (n=10; Fig. 5) and 403.2 ± 24.5 to 455.0 ± 25.7 Ma at Skiag Bridge (n=32; Fig. 5). Fig. 5 shows a summary of the Ar-Ar data for the authigenic K-feldspar and a probability density diagram for both cement generations.

Scatter within the Ar-Ar data for each generation of cement may potentially be attributed to geological variation. For example, if you consider that K-feldspar overgrowths from the Victory Formation (UK Atlantic Margin) were precipitated over a 30 Ma period (Mark *et al*., 2005), then some Ar-Ar age variation for $P1_C$ and $P2_C$ is expected. The two ages for $P1_C$ and $P2_C$ authigenesis broadly correspond with the Grampian (475 to 467 Ma; Dewey, 2005) and Scandian (435 to 420 Ma; Johnson *et al*., 1985) episodes of the Caledonian Orogeny (Mark *et al*., 2007).

5. DISCUSSION

315 5.1 Resolution of different generations of cement

316

317 Bimodal distributions for minimum fluid entrapment temperatures and salinities
318 corresponding to both $P1_C$ and $P2_C$ at both An-t-Sron and Skiag Bridge, supported by
319 mineral compositional differences (Ba in $P2_C$; Mark *et al*., 2007), show that the Ar-Ar
320 ages from $P2_C$ represent a second episode of authigenesis. If only a single fluid
321 inclusion population were present within both cement generations and there was no
322 change in parent fluid composition (Mark *et al*., 2007), then we would have to
323 consider Ar-loss from $P1_C$ and contamination of zone $P1_C$ with excess Ar as potential
324 mechanisms of producing the observed Ar-Ar age differences between $P1_C$ and $P2_C$.
325 Due to differing parent fluid data and compositions for both generations we can
326 discount these mechanisms.

327

328 5.2 Clay content

329

330 Aggregates of 20 by 100 nm sized crystals are present along subgrain boundaries
331 within $P1_C$ (Fig. 4). These crystals are inferred to be illite from their habit and the
332 findings of illite in two previous TEM studies of K-feldspar overgrowths from the UK
333 (Worden & Rushton, 1992; Lee & Parsons, 2003). The replacement of K-feldspar by
334 illite, or passive precipitation of illite within pores (processes which occur post-
335 precipitation of the authigenic K-feldspar; Lee & Parsons, 2003) may potentially
336 affect Ar-Ar ages because illite also contains ^{40}K that will radiogenically decay to
337 $^{40}Ar^*$. However, considering the amount of illite present along subgrain boundaries,
338 the K-ratio between illite and K-feldspar and placing both of these factors in context
339 with the amount of material ablated in order to obtain a single $P1_C$ Ar-Ar age (whole

340 overgrowths), the input of $^{40}Ar^*$ from clay (< 0.1 %) would have had a minimal effect
341 on the Ar-Ar data relative to the error range determined for each individual Ar-Ar age
342 (see Ar-Ar tables in Mark *et al*., 2007).
343
344 5.3 Excess Ar and fluid inclusions
345
346 We have to consider if excess Ar within fluid inclusions which were ablated during
347 Ar-Ar age determination could have influenced the true age of the two cementing
348 generations. We did not directly analyse fluid inclusions for the presence of excess
349 Ar, we used basic modelling.
350
351 Inclusions containing fluids of deep crustal origin often contain between 0.1 and 10
352 ppm excess Ar (Kelley, 2002). Therefore, ablation of fluid inclusions within
353 authigenic K-feldspar overgrowths may have had varying effects upon the final
354 isotopic Ar-Ar age of the mineral, depending on the volume fraction of the inclusions
355 that have been ablated. Fluid inclusions within $P1_C$ and $P2_C$ at Skiag Bridge and An-t-
356 Sron are sparse and range in size from 3-6 µm and 4-9 µm, respectively (Mark *et al*.,
357 2007). Calculations show that if the fluid content of the ablation areas was 1 volume
358 %, and parent fluids contained 0.1 ppm excess Ar, then K-feldspar would exhibit an
359 Ar-Ar age increase of 0.35 Ma. If the same 1 volume % parent fluids contained 10
360 ppm excess Ar, the associated Ar-Ar age increase would be 35 Ma. However, because
361 fluid inclusion volumes, their occurrence and distributions varies between different K-
362 feldspar overgrowths within both samples, and the Ar-Ar ages for each cement
363 generation remain consistent, we suggest that excess Ar within fluid inclusions is not
364 a significant contributing factor. Furthermore, the two samples come from sites that

365 are 30 km apart and it seems highly unlikely that the two samples could have
366 experienced identical excess Ar histories thereby producing similar Ar-Ar ages for
367 both generations of K-feldspar. Additionally, variations in $^{38}Ar_{Cl}/^{39}Ar_K$ which is a
368 proxy for Cl/K ratio and used as an indicator of brine-borne excess Ar (Harrison *et al.*,
369 1994), show no correlation with Ar-Ar age (Mark *et al.*, 2007).
370
371 5.4 ^{39}Ar recoil and sample heating during irradiation
372
373 Recoil loss of ^{39}Ar during irradiation has to be eliminated as a potential process that
374 could result in scattering of the Ar-Ar ages for both $P1_C$ and $P2_C$. ^{39}Ar has a recoil
375 distance of ~ 0.1 µm (Onstott *et al.*, 1995; Villa, 1997). With respect to subgrain sizes
376 for the $P1_C$ microtexture, 15 and 2-3 µm, recoil loss of ^{39}Ar would not be sufficient to
377 explain Ar-Ar age distributions. In $P2_C$ microtextures that contain 0.5-1 µm subgrains,
378 ^{39}Ar recoil is potentially a problematic issue. However, as the ablation areas were
379 maximised (a minimum 50 μm^2), any potential effect of ^{39}Ar movement by ~0.1 µm
380 was negated by the analytical process.
381
382 Sample heating during irradiation of cadmium shielded samples can potentially
383 induce significant Ar-loss. Both wafers were irradiated at different times for different
384 durations in different positions of the McMaster reactor. If heating had induced
385 significant Ar-loss in one or both samples, then we would not have obtained
386 comparable data from both samples.
387
388 5.5 Thermally induced Ar-loss and Ar-Ar age resetting
389

In order to test the Ar-Ar ages for resetting, Ar-loss from subgrains was modelled through a series of tectono-thermal histories (Wheeler, 1996). To model this data we have assumed weighted means for the different cementing phases using v. 3.00 of the isoplot/Ex program (Ludwig, 2003). $P1_C$ at An-t-Sron has a weighted mean of 472.3 ± 5.1 Ma (mean square weighted deviation [MSWD] 3.9) and at Skiag Bridge a weighted mean of 467.0 ± 6.0 Ma (MSWD 2.6). $P2_C$ at An-t-Sron has a weighted mean of 435.9 ± 7.3 Ma (MSWD 1.8) and at Skiag Bridge a weighted mean of 430.2 ± 5.1 Ma (MSWD 4.0). Although the data do not conform to a normal distribution (Fig. 5), with the implication there exists scatter due to geological causes, the weighted means represent a first-order acceptable approximations for the ages of the two episodes of authigenesis for use in Ar diffusion modelling.

The temperatures experienced by the Fucoid Beds during Moine emplacement (which occurred at ~ 430 to 422 Ma; Dewey, 2005), have been reconstructed using evidence from acritarch coloration index (Downie, 1982), illite crystallinity (Johnson *et al*., 1985) and fluid inclusion analysis (Baron *et al*., 2003; Mark *et al*., 2007). Minimum temperatures experienced by the sampled sections of the Fucoid Beds during Moine emplacement are ~200 °C. The thermal data was entered into a simplified tectono-thermal thrust model (Oxburgh & Turcotte, 1974). A simplified thrust model is sufficent to model Ar-diffusion and the maximum palaeotemperature and duration of heating (along with the effective diffusion dimension) are the main controls on Ar diffusion.

5.5.1 Ar-diffusion model

415 The Ar-diffusion model uses forward projection to test the Ar-Ar ages by establishing
416 a thermal history (Wheeler, 1996) against which assumed Ar-Ar 'growth ages' can be
417 evaluated in terms of Ar-loss. In the model, 0 Ma corresponds to ages of authigenesis
418 for both generations of authigenic K-feldspar (~470 and 432 Ma for $P1_C$ and $P2_C$,
419 respectively), and 470 and 432 Ma in the model correspond to the present day for $P1_C$
420 and $P2_C$, respectively. Prior to thrust sheet emplacement at 430 Ma, the model
421 assumes that the temperature in the Fucoid Beds is represented by the fluid
422 entrapment temperatures that were determined previously (90 and 128 °C for $P1_C$ and
423 $P2_C$, respectively; Mark *et al*., 2007). Note that $P2_C$ is younger and contains smaller
424 subgrains than $P1_C$. Therefore, although small $P2_C$ subgrains appear have lost less Ar
425 than larger $P1_C$ subgrains in some instances, $P1_C$ was subjected to an extra 30-40 Ma
426 of heating pre-thrusting.
427
428 *5.5.1.1 8 Ma, 200 °C thermal event.* During thrust sheet emplacement (thrusting
429 inferred to start at 430 Ma; Johnson *et al*., 1985; Kinny *et al*., 1999), a stepped
430 gradient developed within the footwall and the temperature at the thrust sheet-footwall
431 interface was 0.5T (200 °C), where T is the temperature at the thrust sheet base prior
432 to emplacement (~ 400 °C). Rapid thermal re-equilibration of the footwall occurred as
433 heat was conducted away from the thrust front (Johnson *et al*., 1985) through the
434 over-thrusted successions. The footwall cooled from palaeo-maximum temperatures
435 (~ 200 °C) in response to syn- and post-uplift erosion. Assuming a standard erosion
436 rate of 1 km/Myr for a continent-continent collision (current Himalaya erosion rates
437 of 2.1 to 2.9 mm/yr; Galy & France-Lanord, 2001) and a geothermal gradient of 30
438 °C/km, the Fucoid Beds cooled to 150 °C by 422 Ma. We infer a simple linear cooling
439 trend from 422 Ma to present day, and an approximated temperature of 10 °C to

represent the current Fucoid Bed surface temperature. It is important to note that much of the recent Fucoid Bed temperature-time path has had insignificant effects on the diffusion of Ar in the K-feldspar subgrains (Fig. 6).

Diffusion domain sizes determined from TEM work were used to represent the effective diffusion dimensions (Dodson, 1973; subgrains equated to spheres and corresponding radii determined from Fig. 4). $P1_C$ is relatively featureless and has large subgrains (~15 µm in diameter) adjacent to the detrital grain-overgrowth boundary and smaller subgrains (~3 µm diameter) further from the boundary (Fig. 4A-B). From TEM observations and cooling rates calculated using the tectono-thrust model outline above (Fig. 6; 430-422 Ma = 6.25 °C/Ma; and 422-present day = 0.33 °C/Ma), it is possible to calculate the theoretical closure temperatures of the K-feldspar subgrains within the Fucoid Bed samples (Dodson, 1973). 15 and 3 µm subgrains respectively have theoretical closure temperatures of 200 and 212 °C, and 155 and 170 °C for cooling rates of 0.33 and 6.25 °C/Ma. Subgrains are smaller (~1 µm) and more abundant, but irregularly distributed within the $P2_C$ cements (Fig. 4D-F). 1 µm subgrains have a T_c of 143 and 154 °C for cooling rates of 0.33 and 6.25 °C/Ma. Ar-diffusion models were run to quantitatively determine the amount of Ar-loss from both cement generations.

The Ar-diffusion model (Fig. 7) indicates that the 3 µm subgrains will have lost 33 % of their initial $^{40}Ar^*$ (Table 1), and so will yield Ar-Ar ages 140 Ma younger than the growth age. The 15 µm subgrains will have lost 28 % of their $^{40}Ar^*$ and will have yielded Ar-Ar ages 120 Ma younger than the growth age (Table 1). However, because entire $P1_C$ overgrowths were ablated in order to obtain the maximum amount of Ar for

each mass spectrometer measurement, each $P1_C$ Ar-Ar age is a function of variable ratios of 3 µm and 15 µm subgrains. The FIB-TEM method enables examination of only small regions of the authigenic K-feldspar (15x5 µm foils) and as such, it is not possible to give accurate estimates of the proportion of large to small subgrains ablated for any single Ar-Ar age. Assuming a simple subgrain ratio of 1:1 for 15 and 3 µm subgrains, the model estimates that $P1_C$ has lost 30 % of its $^{40}Ar^*$ and Ar-Ar ages have been reset by ~ 130 Ma. Therefore, the Ar-diffusion model estimates the actual age of $P1_C$ authigenesis to be ~600 Ma. The same Ar-diffusion thermal model used for $P1_C$ (Fig. 6) indicates that 1 µm $P2_C$ subgrains (which are younger than the $P1_C$ subgrains) have lost 32 % $^{40}Ar^*$, resetting the $P2_C$ Ar-Ar age by 127 Ma and thus indicating a 'model' Ar-Ar age for $P2_C$ authigenesis of 559 Ma (Fig. 7).

Comparison of the modelled Ar-Ar ages for 'modelled crystallization' of $P1_C$ (600 Ma) and $P2_C$ (559 Ma) with the depositional age of the Fucoid Beds (518 to 510 Ma; Gradstein *et al*., 2004), indicates discrepancies with the Ar diffusion modelling. The subgrain sizes were measured using TEM (Fig. 4) and are consistent with previous observations (Lee and Parsons, 2003). Therefore either the peak palaeotemperature associated with Scandian thrusting or the duration of heating has been overestimated, thereby overestimating Ar-loss from both cement generations. The impact of reducing both the peak palaeotemperature and the duration of the thermal perturbation can be tested by re-running the Ar-diffusion model using new parameters.

5.5.1.2 Reduced palaeothermal maxima. A second series of Ar-diffusion models (still using a thrust-related heating event at 430 Ma for duration of 8 Ma) were run with peak temperatures set at 180, 160 and 140 °C (Fig. 6). The model results are

summarised in Fig. 7. The lowest maximum palaeotemperature of 140 °C causes little (4 %) ^{40}Ar*-loss from 15 µm subgrains and reduces Ar-Ar ages by only ~ 16 Ma. ^{40}Ar*-loss from 3 µm (7 % ^{40}Ar*-loss) and 1 µm (9 % ^{40}Ar*-loss) subgrains, thereby producing widely scattered Ar-Ar ages that are reduced by 27 and 33 Ma, respectively (Table 1).

Despite a geographical separation of 30 km between the two sampling sites, the two generations of cement in both samples have similar Ar-Ar age distributions, implying that $P1_C$ and $P2_C$ Ar-Ar ages at both sites have lost exactly the same amounts of ^{40}Ar* (i.e. experienced identical thermal histories resulting in equal resetting of both samples). In order for authigenic K-feldspar at both sites to have been reset identically, the thrust induced increase in thermal gradient must have been synchronous and uniform over the 30 km distance between the sites as any variation in temperature or timing, would have resulted in different thermal histories and hence, different Ar-Ar ages. Thermal synchronicity between the two sites is not consistent with field and laboratory data.

Dewey (2005) showed that the impingement of the colliding landmasses during the Scandian episode of the Caledonian Orogeny occurred first in the south and resulted in the northern sector of the colliding landmass swivelling into the Laurentian margin. Thrusting was not synchronous across the entire 180 km Moine Thrust Zone. Fluid inclusion data (Baron *et al*., 2003; Mark *et al*., 2007) also show that thrust induced heat flow within the Caledonian Foreland was neither synchronous nor uniform. During thrust emplacement, sites in the south (close to Skiag Bridge) were 30 to 40 °C cooler than those in the north (close to An-t-Sron). Data show that equal resetting

of both $P1_C$ and $P2_C$ in both samples is highly unlikely. Furthermore, we know that temperatures reached a minimum of 200 °C in the Fucoid Beds (Downie, 1982; Johnson *et al*., 2005; Baron *et al*., 2003; Mark *et al*., 2007), but modelling of Ar-diffusion in line with a thermal history depicting peak temperatures of 200 °C and transient heating from the hanging wall into the footwall, clearly overestimates Ar-loss thereby dating the first episode of authigenesis as pre-deposition.

The evidence therefore suggests, if it is assumed that: (i) the K-feldspar diffusion coefficients are correct (Foland, 1974), (ii) there was transient heating to 200 °C and, (iii) subgrain size is representative of the effective diffusion dimension, that the Ar-Ar ages are incompatible with the geological context of the rocks. The other parameter in the Ar diffusion model that can be modified to compensate for the Ar-Ar age overestimation is the mechanism by which heat is removed from the thrust zone and hence, the duration of thrust-induced heating.

5.5.1.3 Short term heating. The alternative heat flow model to transient heating would be very short thermal pulsing of large volumes of hot fluids through the rock, a similar mechanism to which has been observed in Himalayan thrust zones (Le Fort, 1981; Copeland *et al*., 1991). As we know that fluids attained a temperature of 200 °C, the implied periods of fluid flushing removing heat from the thrust zone are short, perhaps in the order of ~10 Ka. The Ar diffusion model was re-run and modified to incorporate short term heating to 200 °C over 10 Ka for $P1_C$ and $P2_C$ (Fig. 8). The model shows that $P1_C$ 15 µm subgrains would lose 4 % $^{40}Ar^*$ and 3 µm subgrains would lose 6 % $^{40}Ar^*$, whilst $P2_C$ 1 µm subgrains would lose 4 % $^{40}Ar^*$ (Fig. 9). Assuming a 1:1 subgrain ablation ratio for $P1_C$ subgrains (15 and 3 µm), Ar-Ar ages

would have been reset by ~ 20 Ma, and $P2_C$ Ar-Ar ages by 17 Ma. The new model shows that the degree of age resetting due to thermally induced Ar-loss by rapid flushing of fluids is consistent with the observed variability of the authigenic K-feldspar Ar-Ar ages (section 4.3). Although the re-run Ar diffusion model incorporating short term heating by fluids is consistent with the observed Ar-Ar ages for both generations of authigenic K-feldspar at both sites, the simplicity of the thermal model depicting short term heating by fluids in the Himalaya has been questioned. Harrison *et al*. (1997) suggested that other factors may be acting in association with short term heating by fluids to influence heat flow within the Himalayas.

In summary, a tectono-thermal model assuming transient heating to 200 °C is incompatible with the Ar-Ar ages of the two generations of K-feldspar cement relative to the age of deposition for the Fucoid Beds. Transient heating to lower temperatures is inconsistent with the regional geology. A tectono-thermal model invoking rapid removal (in the order of 10 Ka) of heat from the thrust zone via flushing of hot fluids is consistent with the Ar-Ar age data and the regional context of the samples, but the validity of the tectono-thermal model has been questioned (Harrison *et al*., 1997). We have assumed for all of the above models that subgrain size is indicative of the effective diffusion dimension. This assumption is based on the fact that dislocation rich subgrain boundaries in authigenic K-feldspar act as fast diffusion boundaries (zero Ar concentration) for $^{40}Ar^*$ as they do in superficially similar patch perthite (Burgess *et al*., 1992). What if this is an incorrect assumption?

5.6 Subgrain microtextures and the effective diffusion dimension

565

566 In order to answer fundamental questions regarding the magnitude and mechanisms of
567 Ar-loss from authigenic K-feldspar, what this paper sets out to address, it is pertinent
568 to consider the properties of superficially similar patch perthite microtextures within
569 deuterically altered alkali feldspars from plutonic igneous rocks (Fig. 1). Direct
570 comparisons have been made between the Ar retention properties of these
571 microtextures and authigenic K-feldspar (Lee & Parsons, 2003). Patch perthites form
572 by deuteric/hydrothermal alteration of strain-controlled exsolution microtextures
573 (unzipping reactions; Parsons & Lee., 2005) and are composed of aggregates of sub-
574 μm to μm-sized subgrains. Microporous patch perthites form veins of networks that
575 develop as fluids have penetrated the grain interior (Fig. 1). As a consequence,
576 deuterically altered alkali feldspars are highly permeable in zones where
577 recrystallization has occurred (Worden *et al*., 1990). Burgess *et al*. (1992) showed that
578 these volumes of recrystallized alkali feldspar lose significant volumes of Ar over
579 time.

580

581 Patch perthite subgrains are typically incoherent and so their boundaries are
582 dislocation-rich (Worden *et al*., 1990). As a consequence, it has been suggested that
583 short-circuit diffusion, which takes place at a rate 4-5 orders of magnitude greater
584 than lattice volume diffusion (Wartho *et al*., 1999), must be the principle mechanism
585 of Ar-loss from patch perthites and not volume diffusion (Lee, 1995). Whereas most
586 alkali feldspars from slowly cooled igneous rocks have discrete patches or veins of the
587 subgrain-rich microtexture (Parsons *et al*., 1999), entire authigenic K-feldspar
588 overgrowths are composed of subgrains (Worden & Rushton, 1992; Lee & Parsons,
589 2003; Mark *et al*., 2005; Mark *et al*., 2006). Hence we assume that at very low

590 temperatures, subgrained authigenic K-feldspar will leak Ar (Lee & Parsons, 2003).
591 Therefore, depending on the thermal history of its parent rock, authigenic K-feldspar
592 Ar-Ar ages may record isotopic closure rather than the crystallization. However,
593 results of previous Ar-Ar studies investigating authigenic K-feldspar (Hagen *et al.*,
594 2001; Mark *et al.*, 2005; Sherlock *et al.*, 2005), suggest that there must be
595 fundamental differences between patch perthite and authigenic K-feldspar (Fig. 1 &
596 4) that can account for why the former leaks Ar whereas the latter appears to retain
597 Ar.
598
599 Although volumes of patch perthite appear turbid in thin section, K-feldspar
600 overgrowths are typically uniform and glass-clear in transmitted-light, indicating that
601 authigenic feldspar has a lower density of micropores and inclusions. Furthermore,
602 unlike patch perthite subgrains, authigenic K-feldspar subgrains form during crystal
603 growth (not recrystallization), and there is no reason why micropores should be inter-
604 connected. Thus, if micropores are not connected, short-circuit Ar diffusion will not
605 operate in the same manner as it does in patch perthite. Furthermore, Fitz Gerald *et al.*
606 (2006) have recently observed networks of even smaller pores within alkali feldspars
607 from igneous rocks which could potentially act as additional pathways for rapid
608 diffusion of Ar. These structures are characteristic of the semicoherent exsolution
609 microtextures of perthitic alkali feldspars and so would not be present within the
610 authigenic K-feldspar.
611
612 Given the hypothesised low micropermeability of microporous authigenic K-feldspar,
613 a theoretical model has been formulated to explain why authigenic K-feldspar may
614 (unlike patch perthite) yield meaningful Ar-Ar growth ages. We suggest there is no

615 direct route for the Ar to escape authigenic K-feldspar on the scale of tens or hundreds
616 of microns as micropores are not connected and therefore diffusion cannot operate at
617 enhanced rates in authigenic K-feldspar as it does in microporous/micropermeable
618 patch perthtie (Fig. 10). Once an approximate equilibrium is established between the
619 concentrations of Ar in the subgrains, the micropores and dislocation-rich boundaries,
620 diffusion from the subgrains into the porous regions of the mineral will be controlled
621 by re-equilibration over time (i.e. the Ar is trapped within dislocations, micropores
622 and subgrain boundaries and therefore violates the assumption that such features act
623 as infinite reservoirs with zero concentrations of Ar). Re-equilibration will occur as
624 further Ar within subgrains is produced by radioactive decay and Ar diffuses out of
625 the K-feldspar subgrains via volume diffusion into dislocations, micropores and
626 subgrain boundaries.
627
628 Although short-circuit diffusion of Ar is potentially restricted within authigenic K-
629 feldspar, thus preventing rapid Ar-loss in comparison to patch perthite, lattice volume
630 diffusion still occurs. Contrary to patch perthite, volume diffusion may be the
631 dominant diffusion mechanism. Ar-loss from the overgrowth boundary will still be
632 occurring by volume diffusion and hence we have to model Ar-Ar age data
633 accordingly (Fig. 10). The implications of this theoretical model are that rather than
634 modelling Ar-loss from K-feldspar overgrowths using subgrain sizes determined from
635 TEM images, Ar-diffusion models should use overgrowth thickness as the effective
636 diffusion dimension (Fig. 10).
637
638 We can quantitatively test the theoretical model by re-running the Ar diffusion models
639 with different effective diffusion dimensions. $P1_C$ overgrowths have a maximum

640 thickness of ~ 40 μm and $P2_C$ overgrowths are up to ~ 100 μm thick (Fig. 3). Using a
641 heating event at 430 Ma with duration of 8 Ma and peak temperature of 200 °C (the
642 original Ar-diffusion model; Fig. 6) and effective diffusion dimensions of 40 and 100
643 μm, the Ar-diffusion model was re-run to test the theoretical model outlined in Fig.
644 10. Grains were approximated to spheres (geometry is not a massively significant
645 variable with respect to the effective diffusion dimension and temperature and
646 duration of heating) and no excess Ar was input into the model. Results are shown in
647 Fig. 11. 470 Ma 40 μm thick overgrowths have been reset by 13 Ma (lost 3 % $^{40}Ar^*$)
648 and 432 Ma 100 μm thick overgrowths have been reset by 3 Ma (lost < 1 % $^{40}Ar^*$).
649 The Ar-diffusion model produces data that are consistent (considering that the model
650 used the maximum effective diffusion dimension for $P1_C$ and $P2_C$ and there was a lot
651 of variability in overgrowth thickness) with the determined Ar-Ar ages, thereby
652 supporting a thermal model of transient heating (Fig. 11) that is also consistent with
653 the regional geology.
654
655 It could be argued that the consistency between the model incorporating transient
656 heating to 200 °C and overgrowth thickness as the effective diffusion dimension (Fig.
657 11) with the Ar-Ar age data is due to an overestimation of the true effective diffusion
658 dimensions (i.e. use of grain size rather than subgrain size determined from TEM
659 imaging), especially as previous studies successfully modelled Ar diffusion using
660 subgrain diameter as the effective diffusion dimension (Mark *et al.*, 2005). Although
661 Mark *et al.* (2005) successfully modelled Ar diffusion using subgrain size rather than
662 overgrowth thickness, the rocks were only exposed to low post-growth temperatures
663 following authigenesis (125 °C). Hence, the variation in effective diffusion dimension

664 is not as significant as it is with respect to the Fucoid Bed case study, and had a
665 limited impact on the Ar-loss data.
666
667 **6. CONCLUSION**
668
669 The Ar-Ar ages two generations of Fucoid Bed authigenic K-feldspar ($P1_C$ and $P2_C$)
670 record different stages of mineral growth and have undergone minimal Ar-loss and
671 Ar-Ar age resetting. Two separate models have been proposed, both of which are
672 consistent with the geological context of the samples (heating to a minimum of 200
673 °C) and can account for the apparent robustness of the authigenic K-feldspar with
674 respect to microtextural repetitiveness of Ar: short-term hot fluid flushing (assuming
675 subgrain sizes are appropriate estimations of the effective diffusion dimension) and
676 transient heating (assuming overgrowth thickness as an appropriate estimation of the
677 effective diffusion dimension).
678
679 We highlight that although K-feldspar microtextures appear to be microporous, it is
680 potentially micropermeability that is the critical factor with respect to Ar-loss and the
681 ability of a mineral phase to record meaningful Ar-Ar isotopic data. This project is not
682 intended to be the definitive study of Ar-diffusion within authigenic K-feldspar, but
683 provides a suitable starting point for discussions of factors governing the reliability of
684 Ar-Ar dating using authigenic K-feldspar and the importance of understanding Ar
685 trapping mechanisms within different feldspar microtextures. More experimental
686 work is required to develop and test (prove/disprove) the theoretical model outlined in
687 this paper. The collection of quantitative Ar-Ar data from authigenic K-feldspar that

has been exposed to a range of high-temperature settings is required before the validity of the model proposed here can be confirmed.

ACKNOWLEDGEMENTS

This work is supported by the Natural Environment Research Council (NERC) Ocean Margins Project, research grant number: 3220/GL021/GRA0782. We thank Professor Alan Craven for access to the FIB-TEM facilities in Glasgow University and Billy Smith, Colin How, John Still and James Schwanethal for technical assistance. Associate Editor Y. Amelin is thanked for comments leading to improvement of this manuscript. Three reviewers, J.A. Wartho, J.K.W. Lee and G.D. Vincenzo are also thanked for detailed reviews, comments and constructive suggestions.

REFERENCES

Baron, M., Parnell, J. & Bordas Le Floch, N., (2003) Preservation of pre-orogenic palaeofluids within the Caledonides of northwest Scotland, Journal of Geochemical Exploration, 78-79, 27-31.

Bowie, S.U.H., Dawson, J., Gallagher, M.J., Ostle, D., Lambert, R.J. & Lawson, R.I., (1966) Potassium-rich sediments in the Cambrian of Northwest Scotland, Transcripts of the Institute of Mineralogy and Metallurgy, 75, B125-145.

Burgess, R., Kelley, S.P., Parsons, I., Walker, F.D.L. & Worden, R.H., (1992) $^{40}Ar/^{39}Ar$ analysis of perthite microstructures and fluid inclusions in alkali feldspars

713 from the Klokken syenite, South Greenland. Earth and Planetary Science Letters, 109,
714 147-167.
715
716 Copeland, P., Harrison, T.M., Hodges, K.V., Maruejol, P., Lefort, P. & Pecher, A.,
717 (1991) An Early Pliocene thermal disturbance of the Main Central Thrust, Central
718 Nepal – implications for Himalayan Tectonics. Journal of Geophysical Research Solid
719 Earth and Planet, 96, 8475-8500.
720
721 Dewey, J.F., (2005) Orogeny can be very short. Proceedings of the National Academy
722 of Science, 102, 15286-15293.
723
724 Dodson, M.H., (1973) Closure temperature in cooling geochronological and
725 petrological systems. Contributions to Mineralogy & Petrology, 40, (3), 259-274.
726
727 Downie, C., (1982) Lower Cambrian acritarchs from Scotland, Greenland and
728 Canada. Transcripts of the Royal Society of Edinburgh, 71, 69-96.
729
730 Fitz Gerald, J.D., Parsons, I. & Cayzer, N., (2006) Nanotunnels and pull-aparts:
731 defects of exsolution lamellae in alkali feldspars. American Mineralogist, 91, 772-
732 783.
733
734 Foland, K.A., (1974) Ar^{40} diffusion in homogeneous orthoclase and an interpretation
735 of Ar diffusion in K-feldspars. Geochimica et Cosmochimica Acta, 38, 151-166.
736

737 Foland, K.A., (1994) Argon diffusion in feldspars. In: Parsons, I., (Eds.) Feldspars
738 and Their Reactions (Kluwer Academic Publishers), 415-447.
739
740 Galy, A. & France-Lanord, C.F., (2001) Higher erosion rates in the Himalaya:
741 Geochemical constraints on riverine fluxes. Geology, 29, 23-26.
742
743 Girard, J.P., Aronson, J.L. & Savin, S.M., (1988) Separation, K-Ar dating and $^{18}O/^{16}O$
744 ratio measurements of diagenetic K-feldspar overgrowths: an example from the
745 Lower Cretaceous arkoses of the Angolan Margin. Geochimica et Cosmochimica
746 Acta, 52, 2207-2214.
747
748 Gradstein, F., Ogg, J. & Smith, A., (2004) A geologic time scale 2004, Cambridge
749 University Press.
750
751 Hagen, E., Kelley, S.P., Dypvik, H., Nilsen, O. & Kjølhamar, B., (2001) Direct dating
752 of authigenic K feldspar overgrowths from the Kilombero Rift of Tanzania. Journal of
753 the Geological Society, London, 158, 801-807.
754
755 Harrison, T.M., Heizler, M.T., Lovera, O.M., Wenji, C. & Grove, M., (1994) A
756 chlorine disinfectant for excess argon released from K-feldspar during step heating.
757 Earth and Planetary Science Letters, 123, 95-104.
758
759 Harrison, T.M., Ryerson, F.J., Le Fort, P., Tin, A., Lovera, O.M. & Catlos, E.J.,
760 (1997) A late Miocene-Pliocene origin for the Central Himalayan inverted
761 metamorphism. Earth and Planetary Science Letters, 146, E1-E7.

762

763 Heaney, P.J., Vicenzi, E.P., Giannuzzi, L.A., Livi, K.J.T., (2001) Focused ion beam
764 milling: a method of site specific sample extraction for microanalysis of Earth and
765 planetary samples. American Mineralogist, 86, 1094-1099.

766

767 Hearn, P.P. & Sutter, J.F., (1985) Authigenic potassium feldspar iin Cambrian
768 carbonates: Evidence of Alleghanian Brine migration. Science, 228, 1529-1531.

769

770 Hearn, P.P., Sutter, J.F. & Belkin, H.E., (1987) Evidence for Late-Paleozoic brine
771 migration in Cambrian carbonate rocks of the central and southern Appalachians:
772 Implications for Mississippi Valley-type sulfide mineralization. Geochimica et
773 Cosmochimica Acta, 51, 1323-1334.

774

775 Johnson, M.R.W., Kelley, S.P., Oliver, G.J.H. & Winter, D.A., (1985) Thermal
776 effects and timing in the Moine Thrust zone. Journal of the Geological Society,
777 London, 142, 863-873.

778

779 Kelley, S.P., Arnaud, N.O. & Turner, S.P., (1994) High spatial resolution $^{40}Ar/^{39}Ar$
780 investigation using an ultra-violet laser probe extraction technique. Geochimica et
781 Cosmochimica Acta, 58, (16), 3519-3525.

782

783 Kelley, S.P., (2002) Excess argon in K-Ar and Ar-Ar geochronology. Chemical
784 Geology, 188, 1-22.

785

786 Kinney, P.D., Strachan, R.A., Friend, C.R.L., Kocks, H., Rogers, G. & Paterson, B.A.,
787 (1999) U-Pb geochronology of deformed metagranites in central Sutherland,
788 Scotland: evidence for widespread late Silurian metamorphism and ductile
789 deformation of the Moine Supergroup during the Caledonian Orogeny. Journal of the
790 Geological Society, London, 160, 259-269.
791
792 Lee, J.K.W., (1995) Multipath diffusion in geochronology. Contributions to
793 Mineralogy and Petrology, 120, 60-82.
794
795 Lee, M.R. & Parsons, I., (2003) Microtextures of authigenic Or-rich feldspar in the
796 Upper Jurassic Humber Group, UK North Sea. Sedimentology, 50, 597-608.
797
798 Lee, M.R., Bland, G.A. & Graham, G., (2003) Preparation of TEM samples by focus
799 ion beam (FIB) techniques: applications to the study of clays and phyllosilicates in
800 meteorites. Mineral Magazine, 67, 581-592.
801
802 Le Fort, P., (1981) Manaslu leucogranite: a collision signature of the Himalaya, a
803 model for its genesis and emplacement. Journal of Geophysical Research, 86, (10),
804 545-550.
805
806 Liu, J., Hay, R.L., Deino, A. & Kyser, T.Y., (2003) Age and origin of authigenic K-
807 feldspar in uppermost Precambrian rocks in the North American Midcontinent,
808 Geological Society of America Bulletin, 115, 422-433.
809

Ludwig, K.R., (2003) Users manual for Isoplot 3.00, a geochronological toolkit for Microsoft Excel. Berkeley Geochronology Centre Special Publication, 4, 54

McDougall, T. & Harrison, M.T., (1999) Geochronology and thermochronology by the Ar/Ar method, Oxford University Press.

Mark, D.F., Parnell, J., Kelley, S.P., Lee, M., Sherlock, S.C. & Carr, A., (2005) Dating of Multistage Fluid Flow in Sandstone. Science, 309, 2048-2051.

Mark, D.F., Parnell, J., Kelley, S.P. & Sherlock, S.C., (2006) Temperature-composition-time (TXt) data from authigenic K-feldspar: an integrated methodology for dating fluid flow events. Journal of Geochemical Exploration, 89, 259-262.

Mark, D.F., Parnell, J., Kelley, S.P. & Sherlock, S., (2007) Resolution of regional fluid flow related to successive orogenic events on the Laurentian Margin. Geology, 35, 547-550

Mark, D.F., Green, P.F., Parnell, J., Kelley, S.P., Lee, M.R., Sherlock, S.C., Late Palaeozoic hydrocarbon migration through the Clair field, West of Shetland, UK Atlantic margin, Geochimica et Cosmochimica Acta (2008), doi: 10.1016/j.gca.2007.11.037

Onstott, T.C., Miller, M.L., Ewing, R.C., Arnold, G.W. & Walsh, D.S., (1995) Recoil refinements: Implications for the $^{40}Ar/^{39}Ar$ dating technique. Geochimica et Cosmochimica Acta, 59, (9), 1821-1834.

836 Oxburgh, E.R. & Turcotte, D.L., (1974) Membrane tectonics and East-African Rift.
837 Earth and Planetary Science Letters, 22, (2), 133-140.
838
839 Parsons, I., (1978) Feldspars and fluids in cooling plutons. Mineral Magazine, 42, 1-
840 17.
841
842 Parsons, I., (1994) Feldspars and their reactions, Kluwer Academic Publishers.
843
844 Parsons, I., Brown, W.L. & Smith, J.V., (1999) $^{40}Ar/^{39}Ar$ thermochronology using
845 alkali feldspars: real thermal history or mathematical mirage of microtexture?
846 Contributions to mineralogy & Petrology, 136, (1-2), 92-110
847
848 Parsons, I. & Lee, M.R., (2000) Alkali feldspars as microtextural markers of fluid
849 flow. In: I. Stober, K. Bucher (Eds.), Hydrogeology of crystalline rocks: Dordrecht,
850 The Netherlands, Kluwer Academic Publishers.
851
852 Parsons, I. & Lee, M.R., (2005) Minerals are not just chemical compounds, The
853 Canadian Mineralogist, 43, 1959-1992.
854
855 Renne, P.R., Swisher, C.C., Deino, A.L., Karner, D.B., Owens, T.L. & DePaolo, D.J.,
856 (1998) Intercalibration of standards, absolute ages and uncertainties in Ar/Ar dating.
857 Chemical Geology, 145, 117-152.
858

Sherlock, S.C., Lucks, T., Kelley, S.P. & Barnicoat, A., (2005) A high resolution record of multiple diagenetic events: Ultraviolet laser microprobe Ar/Ar analysis of zoned K-feldspar overgrowths. Earth and Planetary Science Letters, 238, 329-341.

Smith, C., Lee, M.R. & MacKenzie, M., (2006) New opportunities for nanomineralogy using FIB, STEM/EDX and TEM. *Microscopy and Analysis* 111, 17-20

Spötl, C., Kralik, M. & Kunk, M.J., (1996) Authigenic feldspar as an indication of palaeo-rock/water interactions in permian carbonates of the Northern Calcareous Alps, Austria. Journal of Sedimentary Research, 66, (1), 139-146.

Villa, I.M., (1997) Direct determination of ^{39}Ar recoil distance. Geochimica et Cosmochimica Acta, 61, (3), 689-691.

Walgenwitz, F., Pagel, M., Meyer, A., Maluski, H. & Monie, P., (1990) Thermo-chronological approach to reservoir diagenesis in the offshore Angola Basin: a fluid inclusion, ^{40}Ar/^{39}Ar and K-Ar investigation. The American Association of Petroleum Geologists Bulletin, 74, (5), 547-563.

Walker, F.D.L., Lee, M.R. & Parsons, I., (1995) Microprobes and micropermeable texture in alkali feldspars: geochemical and geophysical implications. Mineral Magazine, 59, 507-536.

883 Warnock, A.C. & van de Kamp, P.C., (1999) Hump-shaped $^{40}Ar/^{39}Ar$ age spectra in
884 K-feldspar and evidence for Cretaceous authigenesis in the Fountain Formation near
885 Eldorado Springs, Colorado. Earth and Planetary Science Letters, 174, 99-111.
886
887 Wartho, J., Kelley, S.P., Brooker, R.A., Carroll, M.R., Villa, I.M. & Lee, M.R.,
888 (1999) Direct measurement of Ar diffusion profiles in a gem-quality Madagascar K-
889 feldspar using the ultra-violet ablation microprobe (UVLAMP). Earth and Planetary
890 Science Letters, 170, 141-153.
891
892 Wheeler, J., (1996) DIFFARG: A program for stimulating argon diffusion profiles in
893 minerals. Computers & Geosciences, 22, (8), 919-929.
894
895 Worden, R.H., Walker, F.D.L., Parsons, I. & Brown, W.L., (1990) Development of
896 microporosity, diffusion channels and deuteric coarsening in perthitic alkali feldspar.
897 Contributions to Mineralogy and Petrology, 104, 507-515.
898
899 Worden, R.H. & Rushton, J.C., (1992) Diagenetic K-feldspar textures: A TEM study
900 and model for diagenetic feldspar growth. Journal of Sedimentary Petrology, 62, (5),
901 779-789.
902
903 **FIGURE CAPTIONS**
904
905 Fig.1: Bright-field TEM image of alkali feldspar grain from the Lower Devonian Shap
906 Granite. The image shows a vein of patch perthite cross-cutting otherwise pristine
907 cryptoperthite. Albite exsolution lamellae in the cryptoperthite are oriented SE-NW in

908 the image and close to (-701) in the corresponding [01-1] SAED pattern. The patch
909 perthite vein comprises a number of subgrains, giving the mottled contrast, and
910 micropores of various sizes (white in the image). Scale bar 1 μm.
911
912 Fig. 2: Simplified geological map of the NW Highlands showing relationship of
913 Caledonian Foreland to Moine Thrust Belt. Sampling sites also shown.
914
915 Fig. 3: Sample shown from An-t-Sron. (A) Backscattered electron SEM image
916 showing generation 1 ($P1_C$) K-feldspar overgrowths on detrital alkali feldspar grains.
917 Generation 2 K-feldspar cement ($P2_C$) envelops $P1_C$ and has occluded remaining
918 porosity. Dol denotes authigenic dolomite and Qz is detrital quartz (After Mark *et al.*,
919 2007). (B) Secondary electron FIB image showing the location of pits excavated using
920 the ion beam into the grain in the upper right of (A). (C) Secondary electron FIB
921 image of a trench prior to lifting out of the foil, which lies between the two crosses.
922 (D) Secondary electron FIB image of the trench following foil removement. (E)
923 SEM-STEM image of a slice on a holey carbon film. The slice comprises feldspar that
924 is thicker on the left and right hand sides than in the central portion, above which is a
925 narrow (~50 nm) layer of gold (white) overlain by the thicker (~1 μm) platinum strap.
926
927 Fig. 4: Samples shown from An-t-Sron. Bright-field TEM images of foils that have
928 been cut and extracted from the grain in Figure 3B. Image A is from trench 2, images
929 B and C are from trench 3 and D, E and F are from trench 4. (A) The interface
930 between the detrital alkali feldspar grain and P1c cement. Mottling in the detrital grain
931 is due to the abundance of dislocations and subgrains and a number of small angular
932 micropores are also present. The authigenic K-feldspar is subgrain-free, has a low

933 defect density and a fine-scale modulated microtexture. The indexed SAED pattern
934 (from the detrital grain) shows that the electron beam is parallel to [312]. Scale bar 1
935 µm. (B) Subgrains (2 to 3 µm in size) within $P1_C$ K-feldspar further from the interface
936 with the detrital grain. Their boundaries (arrowed) have been etched by fluids to form
937 long and narrow pores (arrowed). Scale bar 500 nm. (C) A subgrain boundary within
938 $P1_C$ cement along which have formed clumps of fibrous and poorly crystalline
939 minerals, probably illite. Scale bar 500 nm. (D) P2c cement that contains a number of
940 sub-µm to µm-sized subgrains, all of which have dislocation-rich boundaries. The
941 euhedral subgrains have a {110} adularia habit. Some small micropores have also
942 formed along one of the subgrain boundaries. Electron beam parallel to [001]. Scale
943 bar 1 µm. (E) One subgrain in the P2c cement. Areas of strain contrast highlight
944 dislocations along subgrain boundaries and sub-µm sized angular micropores also
945 occur at subgrain boundaries. Electron beam parallel to [001]. Scale bar 100 nm. (F)
946 Subgrains within P2c cement with more irregular but still dislocation-rich boundaries.
947 Bend countours in the foil help highlight a diffuse microtexture with modulations
948 approximately parallel to a* and b*. Electron beam parallel to [001]. Scale bar 500
949 nm. Note due to a technical failure of the double-tilt axis during TEM examination,
950 the reciprocal lattice directions are not shown in all images.
951
952 Fig. 5: (A) Weighted average plot showing Ar-Ar data for $P1_C$ and $P2_C$ from An-t-
953 Sron and Skiag Bridge (error: 2σ) in relation to Fucoid Bed deposition, the Grampian
954 and Scandian episodes of the Caledonian Orogeny. (B) Relative probability
955 distribution plot for Ar-Ar data from An-t-Sron. (C) Relative probability distribution
956 plot for Ar-Ar data from Skiag Bridge. Both data sets (B&C) show a bimodal
957 distribution suggesting K-feldspar growth from two distinct episodes of authigenesis.

Fig. 6: Diagrams showing reconstructed thermal history, with which K-feldspar subgrains are modelled. The software is a forward modelling program, hence, 0 Ma corresponds to ages of authigenesis, and 470 and 432 Ma correspond to present day. (A) $P1_C$ authigenesis, 200 °C peak temperature. (B) $P2_C$ authigenesis, 200 °C peak temperature. (C) $P1_C$ authigenesis, 180 °C peak temperature. (D) $P2_C$ authigenesis, 180 °C peak temperature. (E) $P1_C$ authigenesis, 160 °C peak temperature. (F) $P2_C$ authigenesis, 160 °C peak temperature. (G) $P1_C$ authigenesis, 140 °C peak temperature. (H) $P2_C$ authigenesis, 140 °C peak temperature.

Fig. 7: Typical DIFFARG output showing modelled response of different sized (15, 3 and 1 µm) subgrains (diffusion domains) to a 200, 180, 160 and 140 °C thermal episode (Fig. 6). The Ar –diffusion model determines the amount of Ar-loss and therefore the degree that each Ar-Ar age is reset, data are summarised in Table 1. (A) $P1_C$ 15 µm subgrain (left: Ar evolution of spherical subgrains of known radius; right: bulk age showing apparent age post exposure). (B) $P1_C$ 3 µm subgrain (left: Ar evolution of spherical subgrains of known radius; right: bulk age showing apparent age post exposure). (C) $P2_C$ 1 µm subgrain (left: Ar evolution of spherical subgrains of known radius; right: bulk age showing apparent age post exposure).

Fig. 8: Diagrams showing short term heated fluid thermal history, against which K-feldspar subgrains are modelled. The software is a forward modelling program, hence, 0 Ma corresponds to ages of authigenesis, and 470 and 432 Ma correspond to present day. (A) $P1_C$ model, 470 Ma to present day. (B) $P2_C$ model, 432 Ma to present day.

983 Fig. 9: Typical DIFFARG output showing modelled response of different sized (15, 3
984 and 1 μm) subgrains (diffusion domains) to a short term fluid heating event, 10,000
985 years at 200 °C (Fig. 6). (A) $P1_C$ 15 μm subgrain (left: Ar evolution of spherical
986 subgrains of known radius; right: bulk age showing apparent age post exposure). (B)
987 $P1_C$ 3 μm subgrain (left: Ar evolution of spherical subgrains of known radius; right:
988 bulk age showing apparent age post exposure). (C) $P2_C$ 1 μm subgrain (left: Ar
989 evolution of spherical subgrains of known radius; right: bulk age showing apparent
990 age post exposure).
991
992 Fig. 10: Simple schematic diagram (not drawn to scale and spheres used to represent
993 subgrains as used in DIFFARG model, true subgrains would have triple-junctions that
994 can not be represented by spheres) showing the fundamental differences between
995 patch perthite (left) and authigenic K-feldspar (right) microtexture. Within both
996 subgrained structures Ar diffusion from the subgrains into the micropores occurs via
997 volume diffusion. However, patch perthite micropores are interconnected and Ar can
998 diffuse out of the micropores via short-circuit diffusion and from the perthite
999 boundary via volume diffusion. Due to a lack of permeability with the authigenic K-
1000 feldspar microtexture, Ar can only diffuse through the grain boundary via volume
1001 diffusion. Short-circuit diffusion within authigenic K-feldspar is reduced. Hence,
1002 whereas currently subgrain size is used as the effective diffusion dimension (A), it
1003 may be more suitable to use the overgrowth thickness (B) to accurately model Ar-
1004 diffusion.
1005
1006 Fig. 11: Typical DIFFARG output showing modelled response of 100 and 40 μm
1007 subgrains to the thermal history shown in Fig. 5.10A&B. Left: Ar evolution of

spherical grains of known radius. Right: bulk age showing apparent age post exposure to the thermal history. Note, DIFFARG is a forward modelling programme, hence for the 100 μm subgrain 0 corresponds to 432 Ma and 432 corresponds to present day. For the 40 μm subgrain 0 Ma corresponds to 470 Ma and 432 Ma corresponds to present day. The model shows that 100 μm subgrains are reset from 432 to 429 Ma and 40 μm subgrains are reset from 470 to 457 Ma.

TABLE CAPTIONS

Table 1: Amount of ^{40}Ar*-loss and Ar-Ar age resetting by thermally activated Ar diffusion.

1019

1020

1021

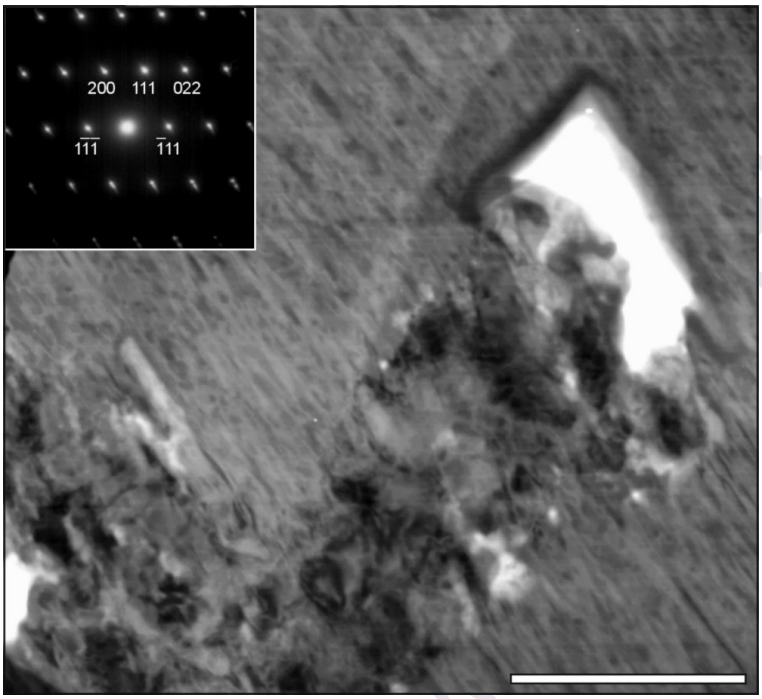

1022

1023

1024

1025

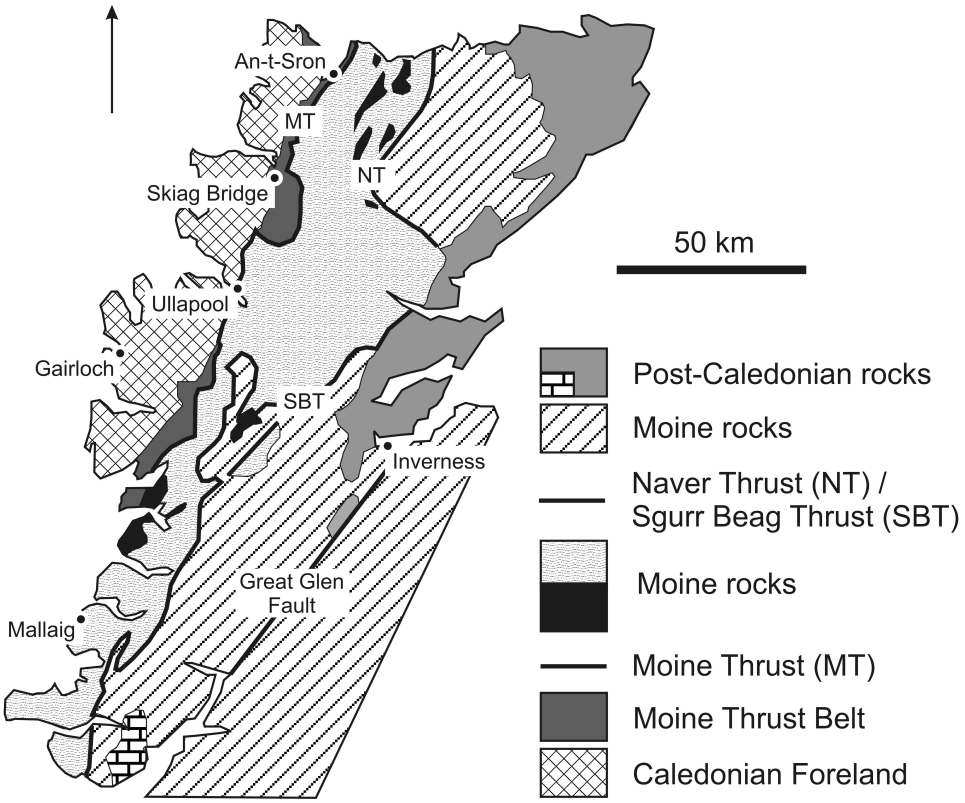

1026

1027

1028

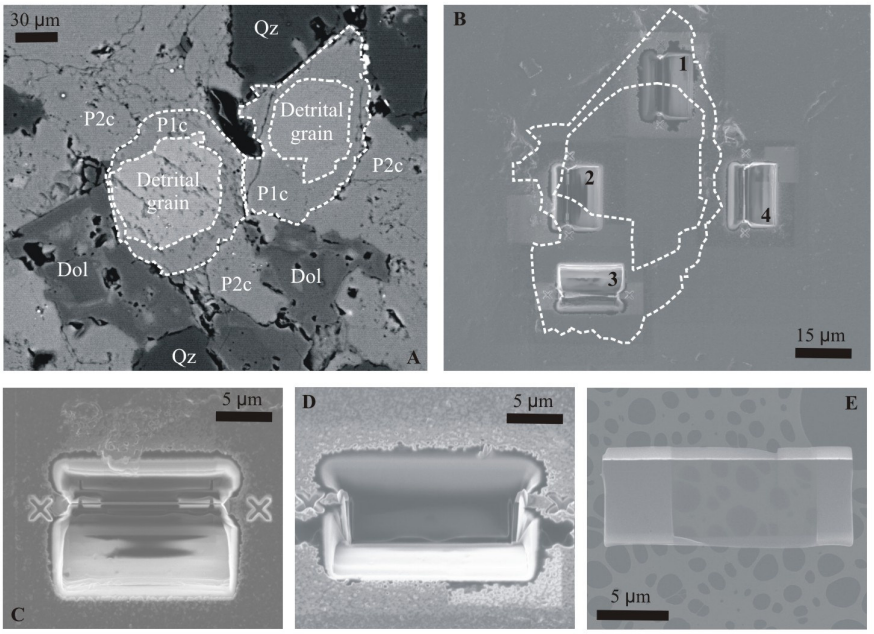

1029

1030

1031

1032

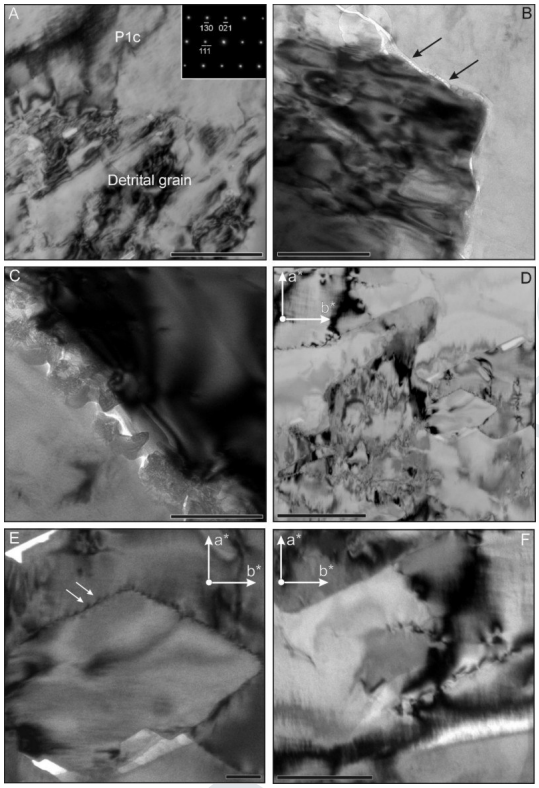

1033

1034

1035

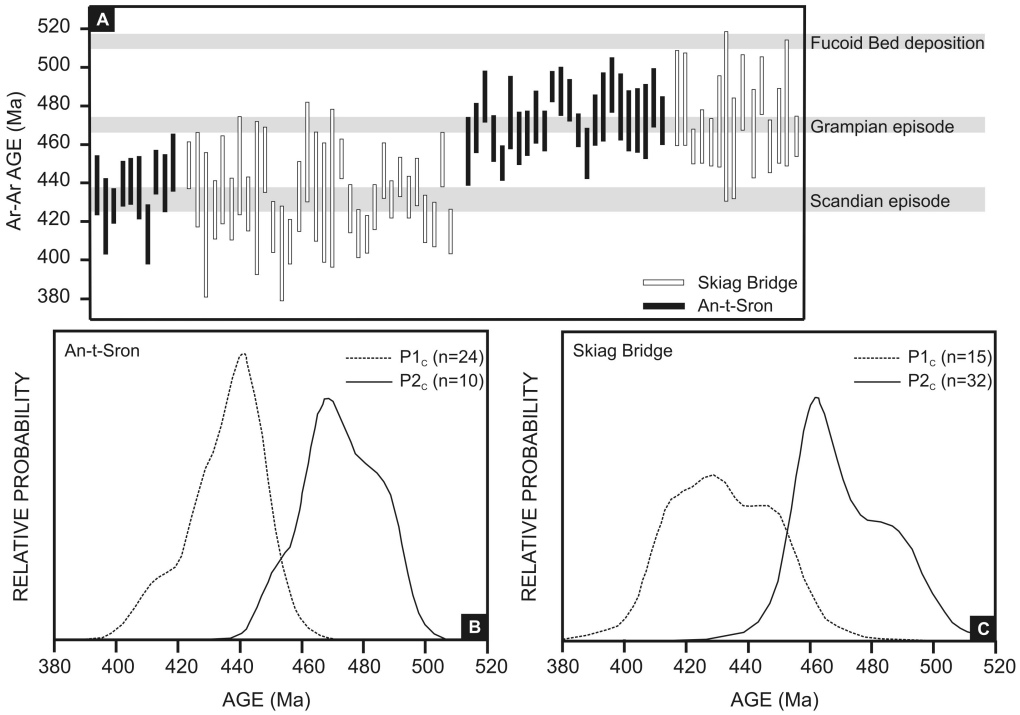

1036

1037

1038

1039

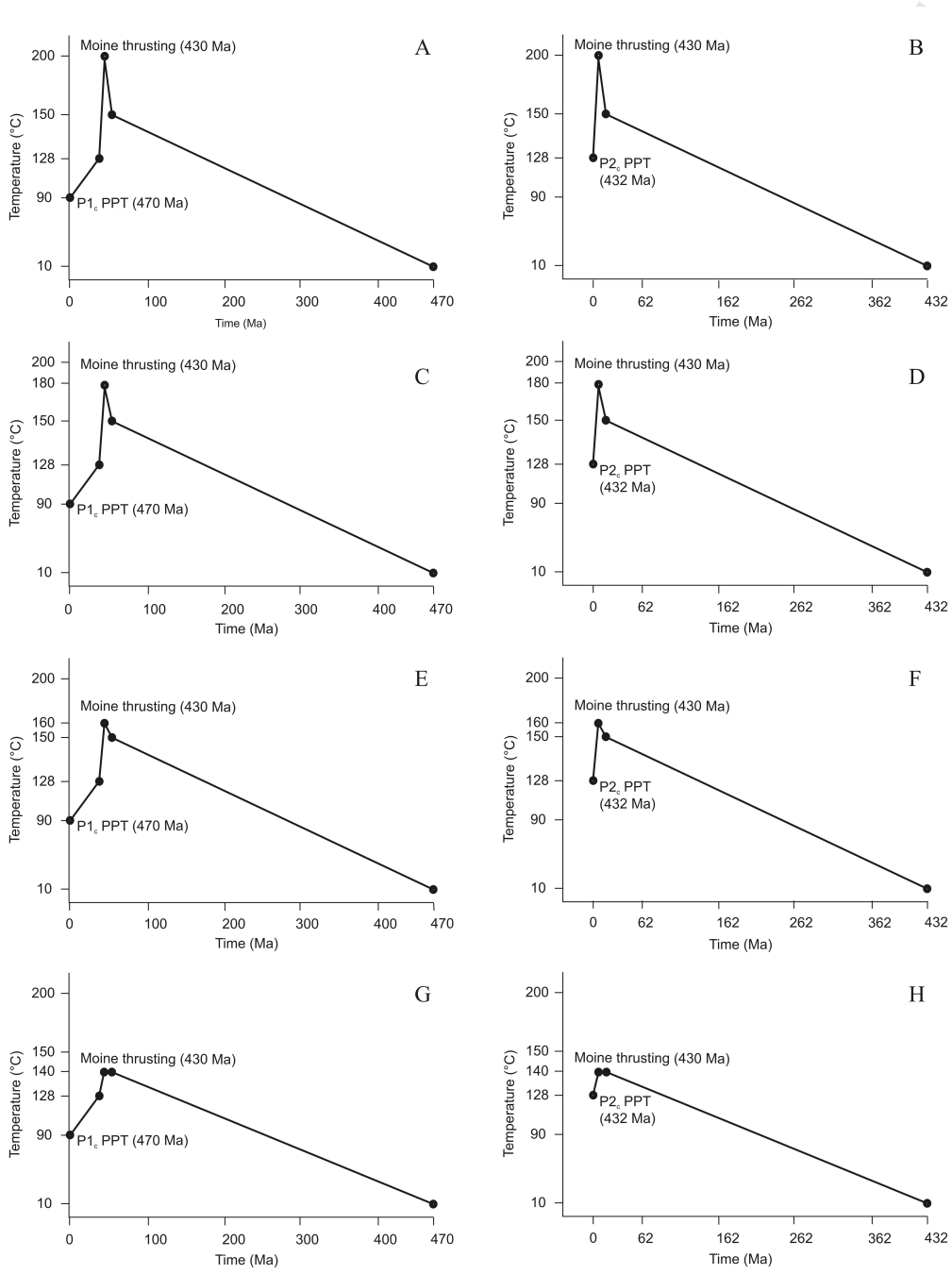

1040

1041

1042

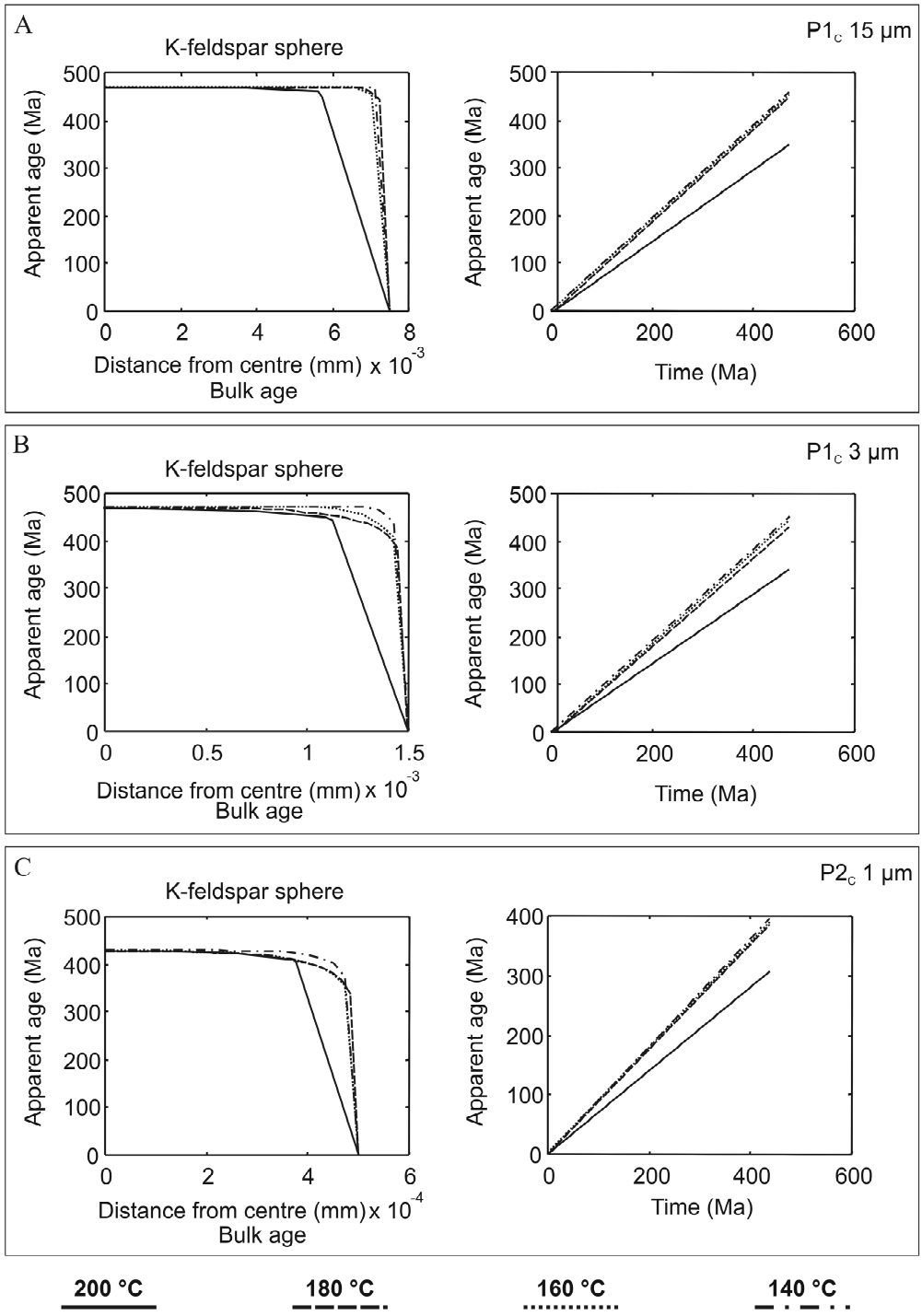

1043

1044

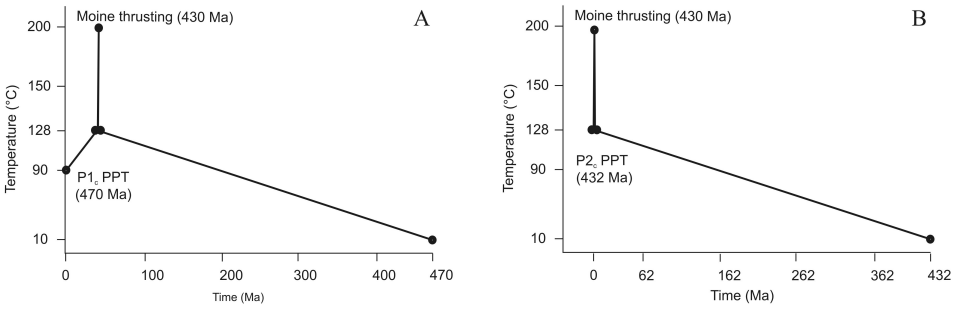

1045

1046

1047

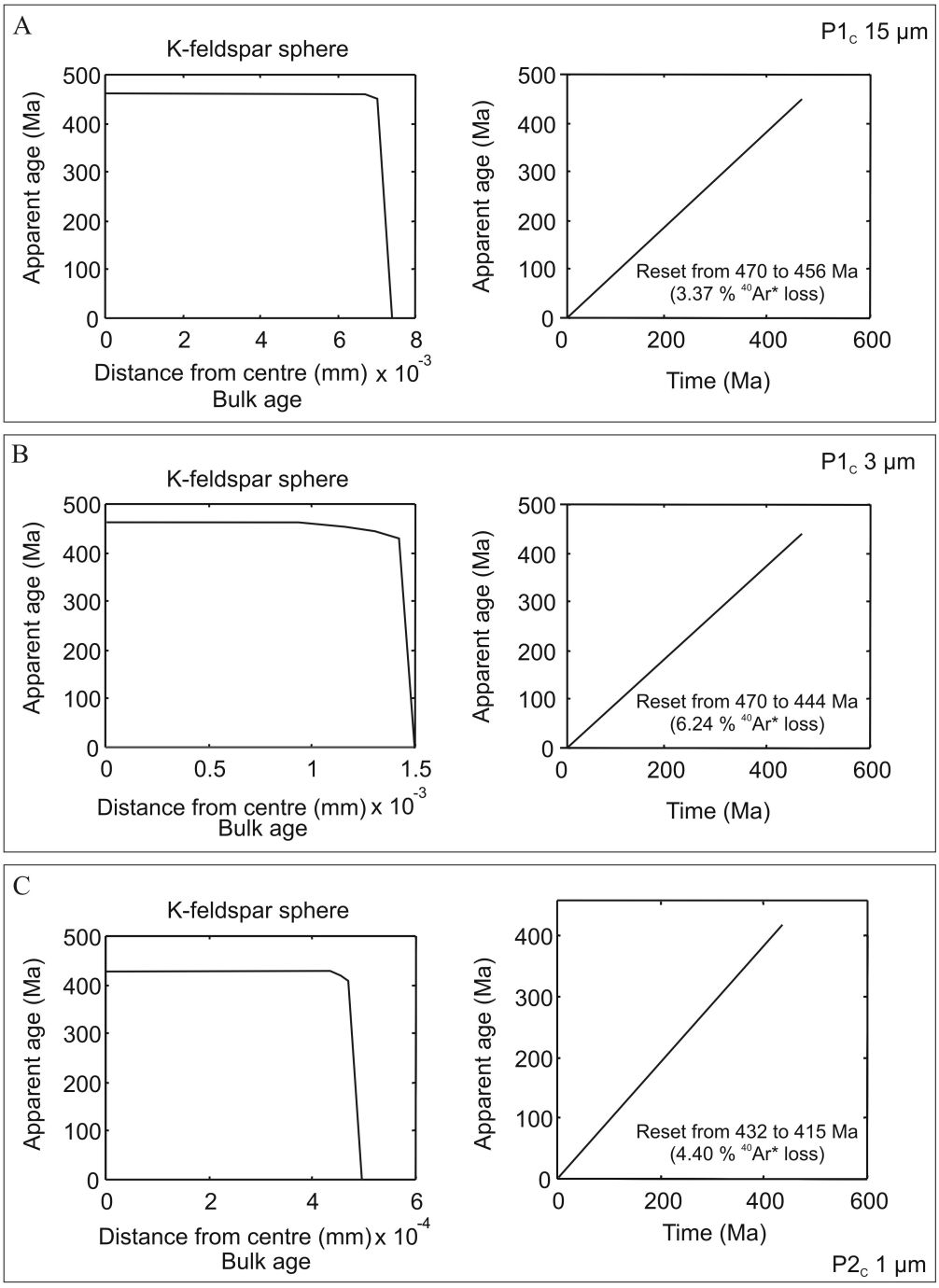

1048

1049

1050

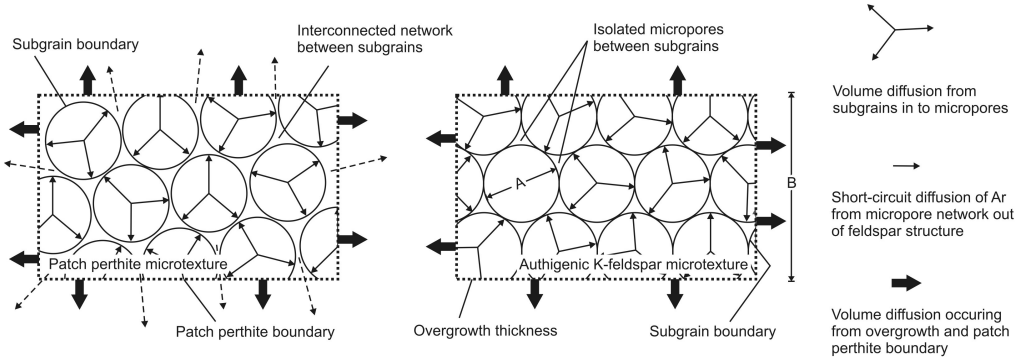

1051

1052

1053

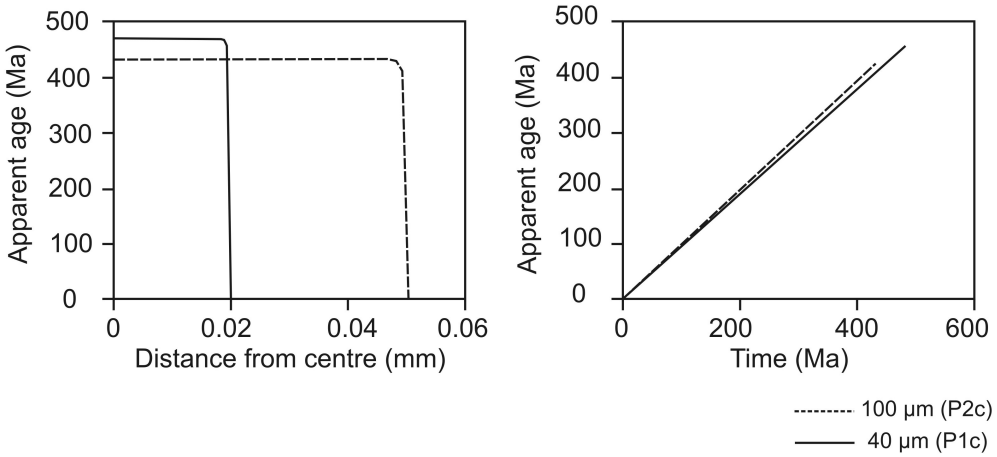

1054

1055

1056

Cement generation	Subgrain size (µm)	Ar-Ar age (Ma)	Peak temperature during thrusting (°C)	Heating duration (Ma)	Ar-loss (%)	Ar-loss (Ma)	Model Ar-Ar age (Ma)
$P1_C$	15	470	200	8	28.1	120.0	350.0
$P1_C$	15	470	180	8	4.8	20.0	450.0
$P1_C$	15	470	160	8	4.3	18.0	452.0
$P1_C$	15	470	140	8	4.0	16.5	453.5
$P1_C$	3	470	200	8	32.6	140.0	330.0
$P1_C$	3	470	180	8	11.9	50.0	420.0
$P1_C$	3	470	160	8	7.4	31.0	439.0
$P1_C$	3	470	140	8	6.5	27.0	443.0
$P2_C$	1	432	200	8	31.9	127.0	305.0
$P2_C$	1	432	180	8	10.8	42.0	390.0
$P2_C$	1	432	160	8	9.8	38.0	394.0
$P2_C$	1	432	140	8	8.6	33.5	398.5

1057